Effects of Sensor Locations on Air-Coupled Surface Wave Transmission Measurements Across a Surface-Breaking Crack

Seong-Hoon Kee and Jinying Zhu

***Abstract*—Previous studies show that the surface wave transmission (SWT) method is effective to determine the depth of a surface-breaking crack in solid materials. However, near-field wave scattering caused by the crack affects the reliability and consistency of surface wave transmission measurements. Prior studies on near-field scattering have focused on the case where crack depth h is greater than wavelength λ of surface waves (i.e., $h/\lambda > 1$). Near-field scattering of surface waves remains not completely understood in the range of h/λ for the SWT method (i.e., $0 \leq h/\lambda \leq 1/3$), where the transmission coefficient is sensitive to crack depth change and monotonically decreases with increasing h/λ. In this study, the authors thoroughly investigated the near-field scattering of surface waves caused by a surface-breaking crack using experimental tests and numerical simulations for $0 \leq h/\lambda \leq 1/3$. First, the effects of sensor locations on surface wave transmission coefficients across a surface-breaking crack are studied experimentally. Data are collected from Plexiglas and concrete specimens using air-coupled sensors. As a result, the variation of transmission coefficients is expressed in terms of the normalized crack depth (h/λ) as well as the normalized sensor location (x/λ). The validity of finite element models is also verified by comparing experimental results with numerical simulations (finite element method). Second, a series of parametric studies is performed using the verified finite element model to obtain more complete understanding of near-field scattering of surface waves propagating in various solid materials with different mechanical properties and geometric conditions. Finally, a guideline for selecting appropriate sensor arrangements to reliably obtain the crack depth using the SWT method is suggested.**

I. Introduction

Surface wave is a type of stress waves that propagates along the surface of a solid. The particle motion amplitude of surface waves exponentially decays with the distance from the free surface boundary. When surface waves propagate across a surface-breaking crack, the low-frequency components of the incident surface waves will transmit to the forward scattering field with attenuation, but the high-frequency components will be reflected back. This property of surface waves is particularly useful to quantitatively evaluate the depth of a surface-breaking crack in a solid medium [1].

Non-destructive testing (NDT) methods of evaluating the depth of a crack based on surface waves has been extensively investigated since the late 1970s. Kino [2], Auld [3], and Achenbach *et al.* [4] developed approximate scattering theories applicable to surface waves to evaluate surface-breaking or near-surface defects. Tien *et al.* [5] investigated the near scattering of surface waves from a surface-breaking crack based on the approximate scattering theory developed by Kino [2], and measured reflection coefficients of incident surface waves to study the behavior of fracture crack extension in ceramics. Jungerman *et al.* [6] explored reflection of surface waves using a pulsed acoustic laser probe to characterize surface defects in an aluminum sample. Cooper *et al.* [7] experimentally investigated surface waves interacting with a surface-breaking crack using non-contact sensors (laser). Achenbach and his colleagues [8]–[10] obtained analytical solutions for investigating near-field scattering of surface waves caused by a surface-breaking crack in solids. They established the relationship between reflection and transmission coefficients of surface waves and the normalized crack depth (crack depth normalized by wavelength of incident surface waves) based on diffraction and scattering of harmonic incident surface waves by a surface-breaking crack in the far-field region (i.e., sensors are located far from a crack opening).

Previous researchers demonstrated that the transmission coefficient of surface waves is a good indicator to estimate the depth of a surface-breaking crack in solid materials. Yew *et al.* [11] experimentally obtained the transmission coefficients of surface waves Tr and normalized crack depth h/λ relation for a surface-breaking crack in aluminum specimens, in which the incident surface waves were generated by dropping a steel ball on the specimen surface. Cheng and Achenbach [12] successfully verified the established Tr and h/λ relation [8]–[10] on aluminum specimens using a self-calibrating ultrasonic technique [13]. Recently, Masserey and Mazza [14] verified that the established Tr and h/λ relation in the studies [8]–[10] is also valid for arbitrary incident waves. For concrete, a heterogeneous but statistically isotropic material, previous researchers [15]–[17] demonstrated that the NDT method based on surface wave transmission (SWT) measurement was effective to evaluate depth of cracks in concrete, even for tightly closed or ill-defined cracks. Recently, Kee and Zhu [18] improved the test consistency and efficiency of the SWT method by using air-coupled sensors.

Near-field scattering caused by the interaction between surface waves and a surface-breaking crack has been investigated by many researchers [18]–[21]. The authors [18]

Manuscript received May 11, 2010; accepted October 25, 2010.

The authors are with the Department of Civil, Architectural, and Environmental Engineering, the University of Texas, Austin, TX (e-mail: jyzhu@mail.utexas.edu).

Digital Object Identifier 10.1109/TUFFC.2011.1820

have found that the near-field scattering significantly affected the consistency of surface wave transmission measurements. Prior studies [19]–[21] on the near-field effect have focused on deep cracks where the depth of crack h is greater than wavelength λ of surface waves (i.e., $h/\lambda > 1$). For the crack depth range used in the SWT method, i.e., $0 < h/\lambda < 1/3$, where the transmission coefficient monotonically decreases with increasing h/λ, the near-field scattering of surface waves is still not fully understood. Yew *et al.* [11] suggested that the location of sensors should be comparable to, or larger than the crack depth to minimize the near-field effect. However, this finding was only based on empirical observation of a narrow range of h/λ. Cheng and Achenbach [12] observed that Tr converged to the far-field analytic solution when sensors were located 5λ from the crack opening. Nevertheless, in field testing, the criteria of 5λ are not always satisfied because of size limitation of structures. Kee and Zhu [18] proposed an approximate criterion for the near-field size, but this conclusion was based on experimental results from only one material, concrete.

In this study, the near-field scattering of surface waves caused by a surface-breaking crack is thoroughly investigated for the crack depth range of $0 < h/\lambda < 1/3$. First, effects of sensor locations on surface wave transmission coefficients across a surface-breaking crack are studied experimentally. Data are collected from Plexiglas and concrete specimens using air-coupled sensors to improve accuracy and test speed. As a result, the variation of transmission coefficients is expressed in terms of the normalized crack depth (h/λ) as well as the normalized sensor location (x/λ). The validity of finite element models is also verified by comparing experimental results with numerical simulations. Second, a series of parametric studies are performed using the verified finite element model to obtain complete understanding of near-field scattering of surface waves in various solid materials with different mechanical properties and geometric conditions. Finally, a guideline for selecting appropriate sensor arrangements to reliably obtain the crack depth using the SWT method is suggested.

II. Experimental Setup

Near-field scattering of surface waves caused by a surface-breaking crack was investigated through a series of experimental tests. The tested materials include a homogeneous material, Plexiglas, and a heterogeneous but statistically isotropic material, concrete. The surface wave transmission functions were obtained using a pair of air-coupled sensors in conjunction with a modified self-calibrating procedure to improve signal consistency and test efficiency.

A. Preparation of Test Specimens

A 1200 × 300 × 25 mm Plexiglas [poly(methyl methacrylate), PMMA] specimen was prepared for surface wave transmission measurements. In this study, the Plexiglas specimen was held in an upright position as shown in Fig. 1. A notch-type crack was created using a hand saw in the Plexiglas specimen, with the crack depth h increasing from 0 to 30 mm in increments of 5 mm, as shown in Table I. In this study, specimens are named based on the material and crack depth, e.g., P5 is a Plexiglas specimen with a crack depth of 5 mm. The hand saw made approximately 0.5-mm-wide cracks, resulting in the width-to-depth ratio smaller than 0.1 for all cracks implemented in this study. According to Masserey and Mazza [14], this value is small enough to neglect the effect of the crack width on transmission coefficients of surface waves, so that the experimental results can be directly compared with the theoretical analysis results. To obtain the phase velocity of surface waves, a dispersion curve was obtained through the multichannel analysis of surface waves (MASW) method [22]. Experimental results showed that the phase velocity converged to 1245 m/s when the frequency is greater than 15 kHz, which agrees with the theoretical value based on the 2-D wave propagation model (i.e., generalized plane stress approximation) by Zerwer *et al.* [23].

Two 800 × 400 × 250 mm concrete specimens were cast in a laboratory. The specimen C0 does not contain a crack, whereas the specimen C20 has a 20-mm deep surface-breaking crack (see Table I). The thickness of these specimens is 250 mm, which is larger than 2 times the

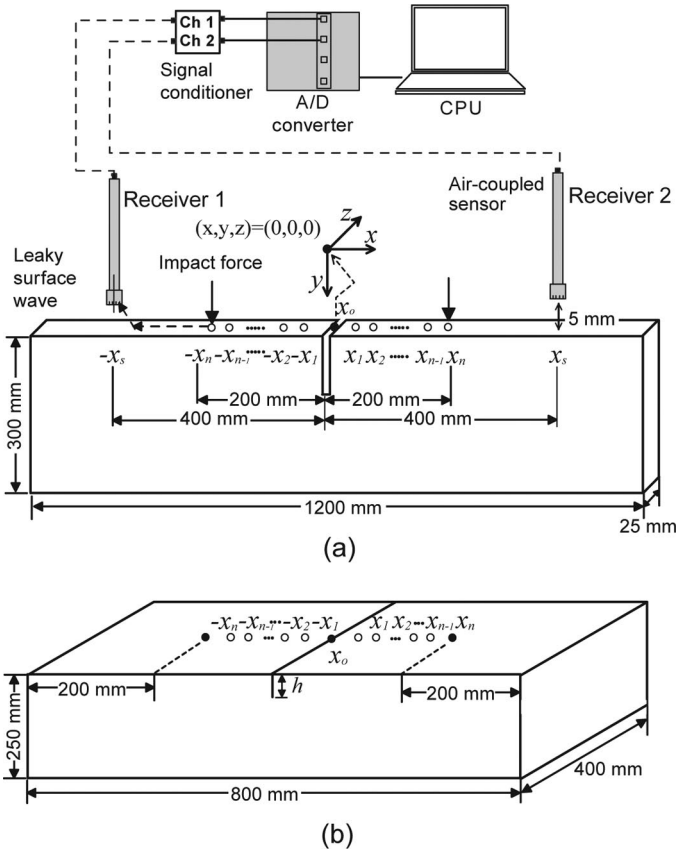

Fig. 1. Experimental setup and data acquisition system for laboratory experiments; (a) Plexiglas and (b) concrete specimens. Note that x_i is a location of an impact source and x_s is a location of a sensor.

TABLE I. SPECIMENS FOR LABORATORY EXPERIMENTS.

Mark	h (mm)	f_c (kHz)	V_R (m/s)	h/λ_c
C0–1	0	17[a]	2200	—
C0–2	0	35[b]		—
C20–1	20	17		0.15
C20–2	20	35		0.32
P0	0	14[c]	1245	—
P5	5			0.06
P10	10			0.12
P15	15			0.18
P20	20			0.24
P25	25			0.30
P30	30			0.36

[a–c]The center frequency f_c was determined through the Fourier transform of incident surface waves generated by dropping a steel ball with diameters of $a = 13$ mm, $b = 8$ mm, and $c = 6.35$ mm.

surface wave wavelength used in this study. Concrete was made of Portland cement type I/II, river sand, and gravel with a maximum size of 10 mm. A notch-type crack with a depth of 20 mm was created in the specimen by inserting a 0.2-mm-thick iron sheet before casting the concrete. The iron sheet was removed from the concrete 12 h later. The density of concrete was 2350 kg/m^3 obtained from the average of five concrete cylinders (10 cm diameter by 20 cm height) cast at the same time as the concrete specimens. The phase velocity of surface waves in concrete is approximately 2200 m/s based on the MASW test when frequency is greater than 10 kHz.

B. Test Setup, Data Acquisition, and Signal Processing

A schematic view of the test setup for the Plexiglas specimens is shown in Fig. 1(a). The test setup of concrete specimens is shown in Fig. 1(b). Two air-coupled sensors (PCB model No. 377B01) were used to measure leaky surface waves propagating on the surface of specimens. Detailed descriptions of the air-coupled sensing technique have been given by Zhu [24].

Previous researchers [13], [16], [17] demonstrated that the self-calibrating procedure was effective for eliminating experimental variations caused by impact sources and receiver coupling in the SWT test. In this study, a modified self-calibrating (MSC) procedure was used to measure the surface wave transmission across a surface-breaking crack from multiple locations (see Fig. 1). In the MSC procedure, an impact point source moves from $-x_n$ to x_n on the specimen surface, and the generated surface waves are recorded by two sensors fixed on both sides of the crack at locations of $-x_s$ and x_s. Note that moving an impact source is more beneficial to test efficiency and signal consistency than moving sensors, especially for contact sensors (e.g., accelerometers). When impact sources are applied at positions $+x_i$ and $-x_i$, the transmission coefficient of surface waves is defined as

$$\mathrm{Tr}(h, x_i) = \sqrt{\frac{\mathbf{V}(x_s, -x_i)\mathbf{V}(-x_s, x_i)}{\mathbf{V}(-x_s, -x_i)\mathbf{V}(x_s, x_i)}}, \tag{1}$$

where $\mathrm{V}(x_s, x_i)$ is the Fourier transform of the signal recorded by the sensor at x_s with the impact source at x_i. Note that (1) is equivalent to the definition given by Achenbach *et al.* [13], Popovics *et al.* [16], and Song *et al.* [17] based on the self-calibrating procedure according to source-receiver reciprocity [25].

In addition, to improve signal consistency, five repeated signal data sets were collected from the same test location. These five transmission functions were then arithmetically averaged in the frequency domain. To evaluate the quality of obtained signals, the signal coherence function defined in (2) was used to check consistency of the signal data:

$$\mathrm{SC}_{12}(f) = \frac{\left|\sum G_{12}(f)\right|^2}{\sum G_{11}(f) \times \sum G_{22}(f)}, \tag{2}$$

where $G_{12}(f)$, $G_{11}(f)$ and $G_{22}(f)$ are the cross-spectrum and auto-spectrum functions between sensor outputs $V(x_s, -x_i)$ and $V(-x_s, -x_i)$ caused by an input at $-x_i$. Similarly, $\mathrm{SC}_{21}(f)$ can also be calculated from signals $V(-x_s, x_i)$ and $V(x_s, x_i)$. The value of $\mathrm{SC}(f)$ ranges from 0 to 1.0. A value close to 1.0 indicates good signal quality and repeatability. Therefore, the signal coherence function can be used to select the acceptable frequency range of a transmission ratio curve.

The measured surface wave transmission coefficient Tr_h was further normalized by Tr_0, which is the transmission coefficient obtained from crack-free regions. This procedure will eliminate material attenuation and the geometric spreading effect caused by a point source. The normalized transmission coefficient Tr_n is defined as

$$\mathrm{Tr}_n(h, x) = \frac{\mathrm{Tr}_h(x)}{\mathrm{Tr}_0(x)}. \tag{3}$$

All analyses were performed in the frequency domain. A Hanning window was applied to the time-domain signals to extract the surface wave component.

For Plexiglas specimens, the transient force was generated by dropping a 6.35-mm diameter steel ball guided by a plastic tube. The impact force generated incident surface waves with a center frequency around 14 kHz, and provided good signal consistency up to 30 kHz. The center frequency of incident surface waves was determined from the Fourier transform of the windowed signal measured in the backward scattering field (see Fig. 2(a) for the specimen P10). For concrete specimens, steel balls with diameters of 13 and 7 mm were used. The center frequencies of the incident surfaces were around 17 and 35 kHz, and the acceptable frequency ranges were up to 35 and 60 kHz, respectively. Fig. 2(b) shows typical received signals corresponding to the center frequency of 17 kHz. The acquired signals were digitized at a sampling rate of 10 MHz using an NI-USB 5133 oscilloscope (National Instruments, Austin, TX).

In Fig. 2(d), it is also noted that signals from reciprocal locations, such as $\mathrm{V}(x_s, x_i)$ versus $\mathrm{V}(-x_s, -x_i)$, and

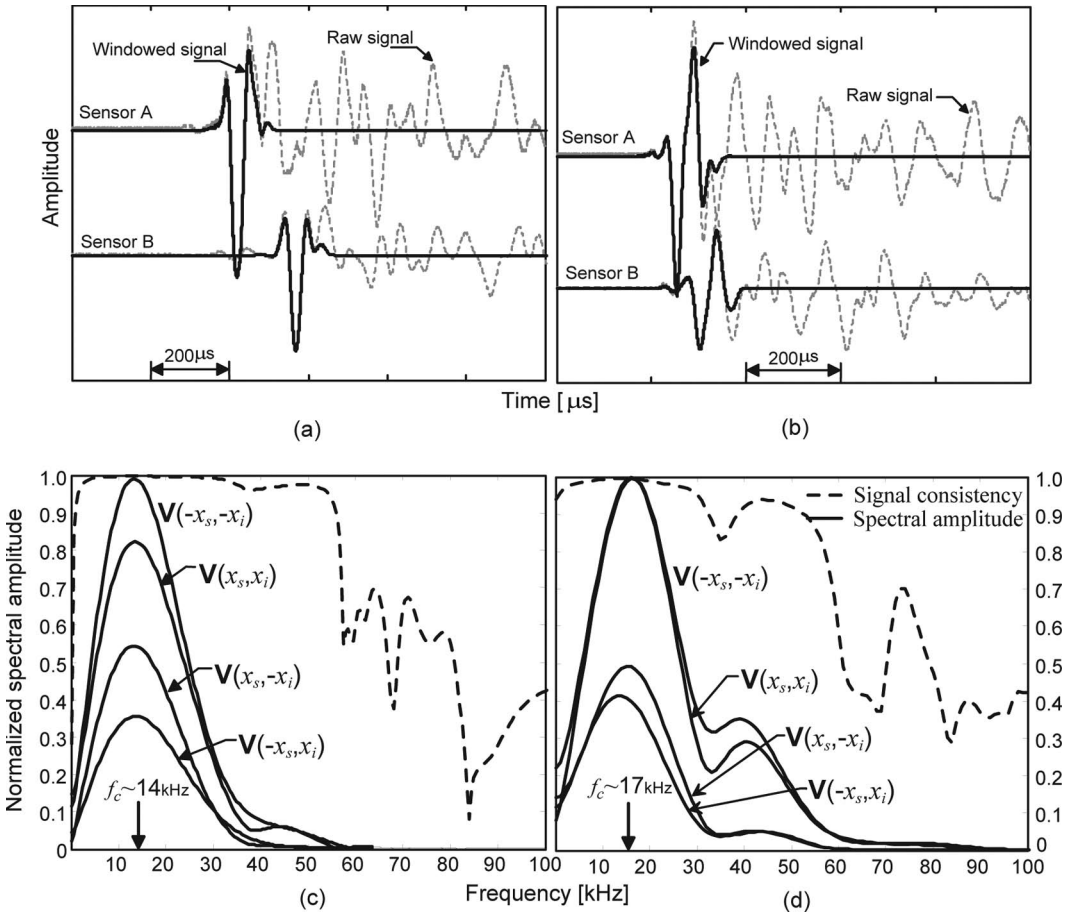

Fig. 2. Typical signal from Plexiglas and concrete specimens: (a) typical time-domain signals from a Plexiglas specimen (P10) using a steel ball with a diameter of 6.35 mm; (b) typical time-domain signal from a concrete specimen (C20) using a steel ball with a diameter of 8 mm; (c) and (d) show normalized spectral amplitude and signal consistency calculated using the windowed signals shown in (a) and (b), respectively.

$V(-x_s, x_i)$ versus $V(x_s, -x_i)$, show good agreement with each other. It indicates the experimental setup is almost symmetric about the center line between two sensors. Signals in Fig. 2(c) show some degrees of asymmetry, but the effects of asymmetry on transmission calculation will be cancelled by using (1).

III. Numerical Simulation

Commercial finite element analysis software (ABAQUS Standard v. 6.7.1) [26] was used to simulate the transient behavior in solids. Although the specimens are better simulated using 3-D models, 2-D models were developed with material properties corresponding to Plexiglas and concrete to save computing time. Each model number actually corresponds to 11 FEM models with the crack depth varying from 0 to 100 mm (see Table II). A small-domain 3-D model was developed to check the validity of 2-D models. A comparison between the 2-D and 3-D models are presented in Section IV-C.

For Plexiglas, a finite element (FE) model (model 10 in Table II) was built using rectangular bilinear plane stress elements (CPS4), as shown in Fig. 3. The mesh size was designed as 5 mm so that at least 10 elements could participate to express the minimum wavelength $\lambda_{\min}$ [27]. In addition, the time increment Δt for integration was chosen to be 1 μs, which is small enough to prevent a propagation of disturbance through a grid size during one time step. The transient impact source was applied on the free surface at the location of $(x, y) = (200, 0)$. The force function of the transient impact point source (see Fig. 3) is

$$f(t) = \begin{cases} \sin^2(\pi t/T), & 0 \le t \le T, \\ 0, & T < t, \end{cases} \tag{4}$$

where T is the duration of impact. Note that the quadratic force function in (4) was verified to be effective for simulating the transient contact forces by previous researchers [28]. Infinite (energy absorbing) boundaries were placed at the outer edge to simulate a solid half-space. Material properties were assumed homogeneous and linear-elastic. This assumption is valid and reasonable within the frequency range in this study, (center frequency $f_c \sim$ 13 kHz). Material properties of the Plexiglas were selected as Young's modulus $E = 5800$ MPa, Poisson's ratio $v = 0.33$, and mass density $\rho = 1200$ kg/m^3. The corresponding velocities of P-, S-, and surface waves were 2328, 1347, and 1240 m/s, respectively.

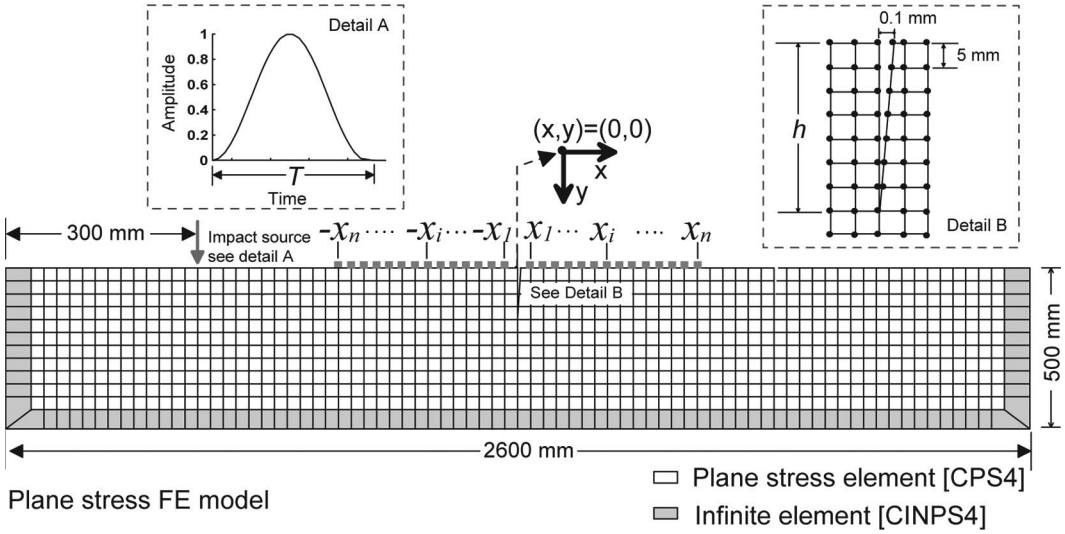

Fig. 3. A finite element model used for numerical simulations of Plexiglas models.

TABLE II. Finite Element Models and Parameters.

Model no.	v	E (GPa)	ρ (kg/m^3)	T (μs)	Element type*	h (mm)
Model 1	0.22	33.6	2400	40	4AX	0, 10,20,30,40,50,
Model 2	0.22	33.6	2400	60	4AX	60,70,80,90,100
Model 3	0.22	33.6	2400	80	4AX	
Model 4	0.22	33.6	2400	100	4AX	
Model 5	0.22	33.6	2400	120	4AX	
Model 6	0.22	33.6	2400	140	4AX	
Model 7	0.33	33.6	2400	60	4AX	
Model 8	0.22	33.6	2400	60	4PS	
Model 9	0.33	5.8	1200	60	4AX	
Model 10	0.33	5.8	1200	60	4PS	
Model 11	0.22	33.6	2400	60	4PE	
Model 12	0.33	5.8	1200	60	C3D8	0, 20

*4AX = 4-node axi-symmetric element; 4PS = 4-node Plane Stress element; 4PE = 4-node plane stain element; and C3D8 = 8-node 3-D element.

For concrete, FE models (models 1–6 in Table II) were built using rectangular bilinear axis-symmetric elements (CAX4) with a mesh size of 5 mm, and time increment of 1 μs according to previous research [18]. The impact force described in (4) was applied at the axis, and the crack is 800 mm from the axis. The material properties were Young's modulus of 33 630 MPa, Poisson's ratio of 0.22, and mass density of 2400 kg/m^3. The corresponding velocities of P-, S-, and surface waves were 4050, 2420, and 2215 m/s, respectively.

In addition, models 7, 9, 10, 11, and 12 were used to investigate the effects of Poisson's ratios and element types. Details are shown in Section IV-C.

IV. Results and Discussion

A. Near-Field Scattering of Surface Waves by a Surface-Breaking Crack

Near-field scattering of surface waves caused by a surface-breaking crack in Plexiglas and concrete was investigated through experimental tests and numerical simulations (FEM). To eliminate the effect of geometric attenuation, the surface response in the near-scattering field of the crack was normalized by the corresponding response in a crack-free model as follows:

$$V_{hn}(x/\lambda, t) = \frac{V_h(x/\lambda, t)}{V_0(x/\lambda, t)}, \tag{5}$$

where $V_h(x/\lambda, t)$ is the out-of-plane component of the surface velocity response in the near-scattering field of the crack with depth h, x/λ is the normalized sensor location from the crack opening (i.e., the distance of sensors from a crack opening x normalized by the wavelength of surface waves λ), and t is time. $V_0(x/\lambda,t)$ is the surface velocity response from a crack-free model. Figs. 4(a) and 4(b) show B-scan images representing surface velocity from FE model 2, which represents two concrete models with a surface-breaking crack with depths of 20 mm ($h/\lambda \sim 0.15$), and 100 mm ($h/\lambda \sim 0.76$), respectively. Consistent with observations from previous researchers [18], [21], mode-converted waves (R_i–R_s–P) as well as transmitted-, and

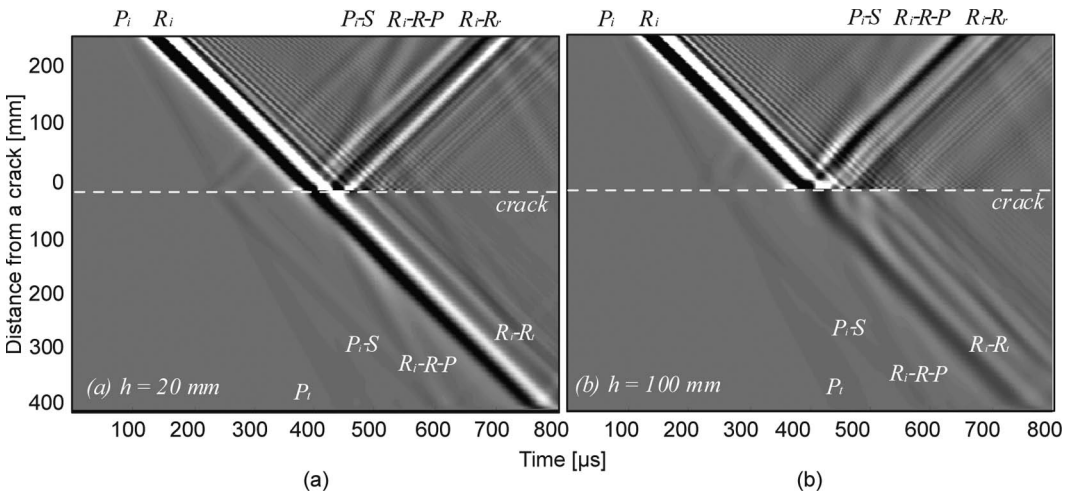

Fig. 4. B-scan image of the near-scattering field of surface waves caused by a surface-breaking crack in FE model 2: (a) $h = 20$ mm ($h/\lambda \sim 0.15$), (b) $h = 100$ mm ($h/\lambda \sim 0.76$). Note that locations of the cracks were denoted by dashed lines.

reflected surface waves (R_i–R_t, and R_i–R_r) are clearly observed in the near-scattering field of surface waves, where R_i, R_t, R_r, and R_s are incident, transmitted, reflected surface waves, and surface skimming waves [21].

To obtain more complete and quantitative properties of the near-field scattering field caused by a surface-breaking crack, the amplification coefficient (APC) curve was defined. It is the peak amplitude ratio between the vertical velocity obtained on a cracked model (V_h) and that on a crack free model (V_0) as follows:

$$\mathrm{APC}(x/\lambda) = \frac{\max(V_h(x/\lambda, t))}{\max(V_0(x/\lambda, t))}. \tag{6}$$

Fig. 5 shows APC versus x/λ curves from experimental and numerical simulation results on Plexiglas specimens, where x/λ is the normalized distance from a crack opening. The experimental data were measured from the Plexiglas specimens P10 ($h/\lambda \sim 0.12$), and P30 ($h/\lambda \sim 0.36$), and the numerical simulation results were from the Plexiglas FE model 10 with crack depths of 10 mm ($h/\lambda \sim 0.12$), and 30 mm ($h/\lambda \sim 0.37$) (refer to Tables I and II). Experimental data from the Plexiglas specimens are presented as solid circles with dashed lines and the numerical simulation results from the FE model 10 are plotted using solid lines. Fig. 5 shows good agreement between the experimental measurements and the numerical simulations. Consistent with previous observations by the authors [18], the APC curves depend on the crack depth h, the wavelength λ, and the distance from the crack x. In the backward-scattering field, APC curves show small oscillation around 1.0. In the forward-scattering field, APC curves decrease sharply from the upper peak at the crack location and then gradually reach a constant value with increasing x/λ. This value can be regarded as the surface wave transmission coefficient in far-field regions. Signal enhancement and oscillations in the near-scattering field can be explained in two ways: 1) particles around a crack are easier to move than the solid region without a crack because of lower stiffness around a surface-breaking crack; and 2) interaction between direct surface waves and mode-converted bulk waves and secondary surface waves results in constructive and destructive interference in the near-field [18], [21].

B. Effect of Sensor Locations on Surface Wave Transmission Measurement

Effects of near-field scattering of surface waves on the surface wave transmission were investigated in the frequency domain. Fig. 6 shows the transmission coefficients versus normalized sensor location x/λ obtained from the Plexiglas specimens in the laboratory experiments. The transmission coefficients calculated at the center frequencies for the Plexiglas specimens P10 ($h/\lambda \sim 0.08$), P15 ($h/\lambda \sim 0.15$), P25 ($h/\lambda \sim 0.24$), and P30 ($h/\lambda \sim 0.31$) are depicted as circles, triangles, squares, and diamonds in Fig. 6. For comparison purposes, the transmission coefficients obtained from the FE model 10 (h/λ of 0.08, 0.16, 0.24, and 0.32) are also shown in Fig. 6 as dashed lines. All transmission coefficients were calculated in the frequency domain as defined in (1) and (3) [16], [17]. Overall, the experimental transmission coefficients obtained from the Plexiglas specimens match well with numerical analysis results. This good agreement verifies the validity of the FE models used in this study. Furthermore, both experimental studies and numerical simulations clearly reveal that the surface wave transmission coefficient depends not only on the depth of a crack and the wavelength of surface waves, but also on the distance of sensors from the crack opening in the near-scattering field. When measurements are taken at points located too close to a crack opening (e.g., x/λ is less than 0.2 to 0.3), the transmission coefficient is significantly higher than those measured in the far-field suggested in [10], [12]. The enhancement of transmission coefficient measurements in the near-scattering field was also pointed out by Richart *et al.* [29]. In addition, the transmission coefficient shows oscillatory behav-

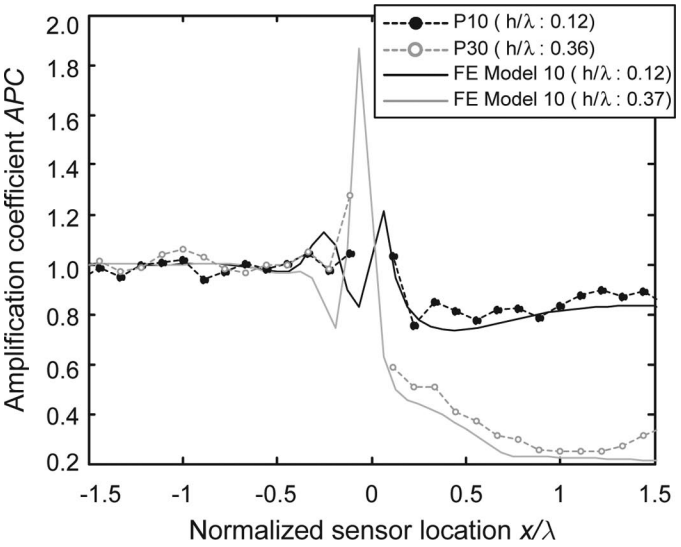

Fig. 5. Amplification coefficient versus the normalized sensor location x/λ obtained from Plexiglas specimens (P10 and P30) and FE model 10.

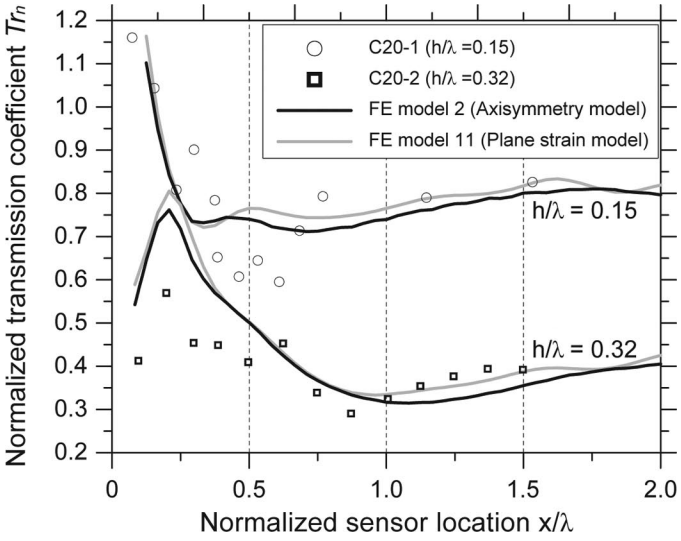

Fig. 7. Transmission coefficient versus normalized sensor location obtained from concrete specimens and FE models 2 and 11.

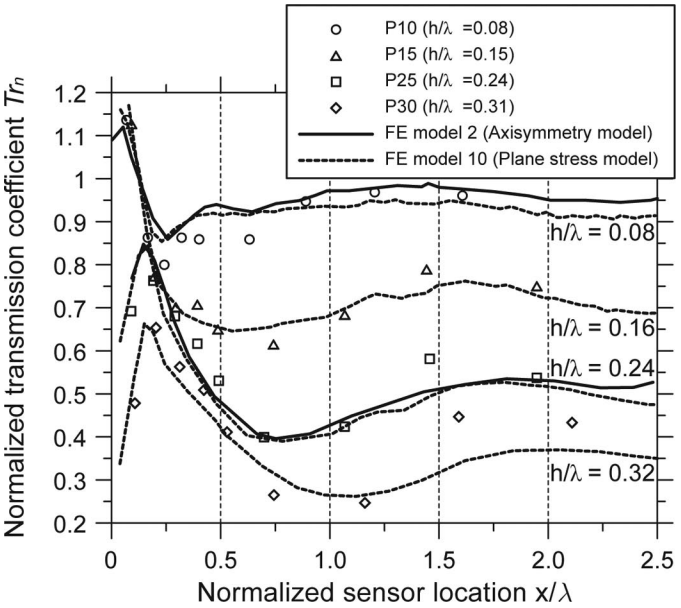

Fig. 6. Transmission coefficients versus normalized sensor location (x/λ = sensor to crack opening distance normalized by the wavelength of incident surface waves) obtained from Plexiglas specimens through laboratory experiments and numerical simulations using FE model 10. For comparison, results from concrete models (FE model 2) are also shown as solid lines.

ior in the near field and gradually converges to a constant value with increasing x/λ ($x/\lambda \sim 2$). Consistent with the observations of prior researchers [10], [14], [30], the normalized crack depth (h/λ) is the most critical parameter to determine transmission coefficients of surface waves in the far-field region.

Fig. 7 shows the transmission coefficients and normalized sensor location x/λ obtained from the concrete specimens. Transmission coefficients were obtained from the concrete specimen of C20-1 using a 13-mm diameter steel ball and C20-2 using an 8-mm steel ball. The corresponding center frequencies are 17 and 35 kHz, and the normalized crack depths are $h/\lambda = 0.15$ and $h/\lambda = 0.32$, respectively. For comparison purposes, $\mathrm{Tr_n}$ calculated from FE Model 2 (black solid lines) and FE Model 11 (gray solid lines) for h/λ of 0.15 and 0.32 are also shown in Fig. 7. Overall, the experimental data show trends similar to the numerical transmission curve, such as 1) enhancement of transmission coefficients for $x/\lambda < 0.5$; 2) oscillation of transmission coefficients with varying sensor location; and 3) convergence to the constant transmission coefficient when x/λ is close to 2. However, the difference between the experimental and numerical transmission curve is larger than that in the Plexiglas case, particularly in the near-field region. This difference might be caused by the inhomogeneity of concrete materials and wave scattering by coarse aggregates, which were not taken into account in the FE models in this study.

C. Parametric Study Based on Numerical Models

To obtain general conclusions of the near field effects, a series of parametric studies were performed using the FE models which were verified in the previous section. The FE models used in the parametric study are summarized in Table II. The main variables are 1) crack depth h, $0 \leq h \leq 100$ mm; 2) duration of impact T, $40 \leq T \leq 140$ μs; 3) Poisson's ratio v of 0.22 and 0.33; and 4) element type of 4-node axisymmetric (4AX), plane stress (4PS), plane strain (4PE) and 3-D brick (C3D8) elements.

Fig. 8(a) shows the $\mathrm{Tr_n}$ and x/λ relations for $h/\lambda =$ 0.11, 0.22, 0.33, and 0.45 obtained from FE Models 1–6, with the impact duration $T = 40$, 60, 80, 100, 120, and 140 μs. Different combinations of T and h give different h/λ values, and one h/λ may correspond to several T and h combinations, as shown in Fig. 8(a). For a given h/λ, all $\mathrm{Tr_n}$ versus x/λ curves converge to a constant value with

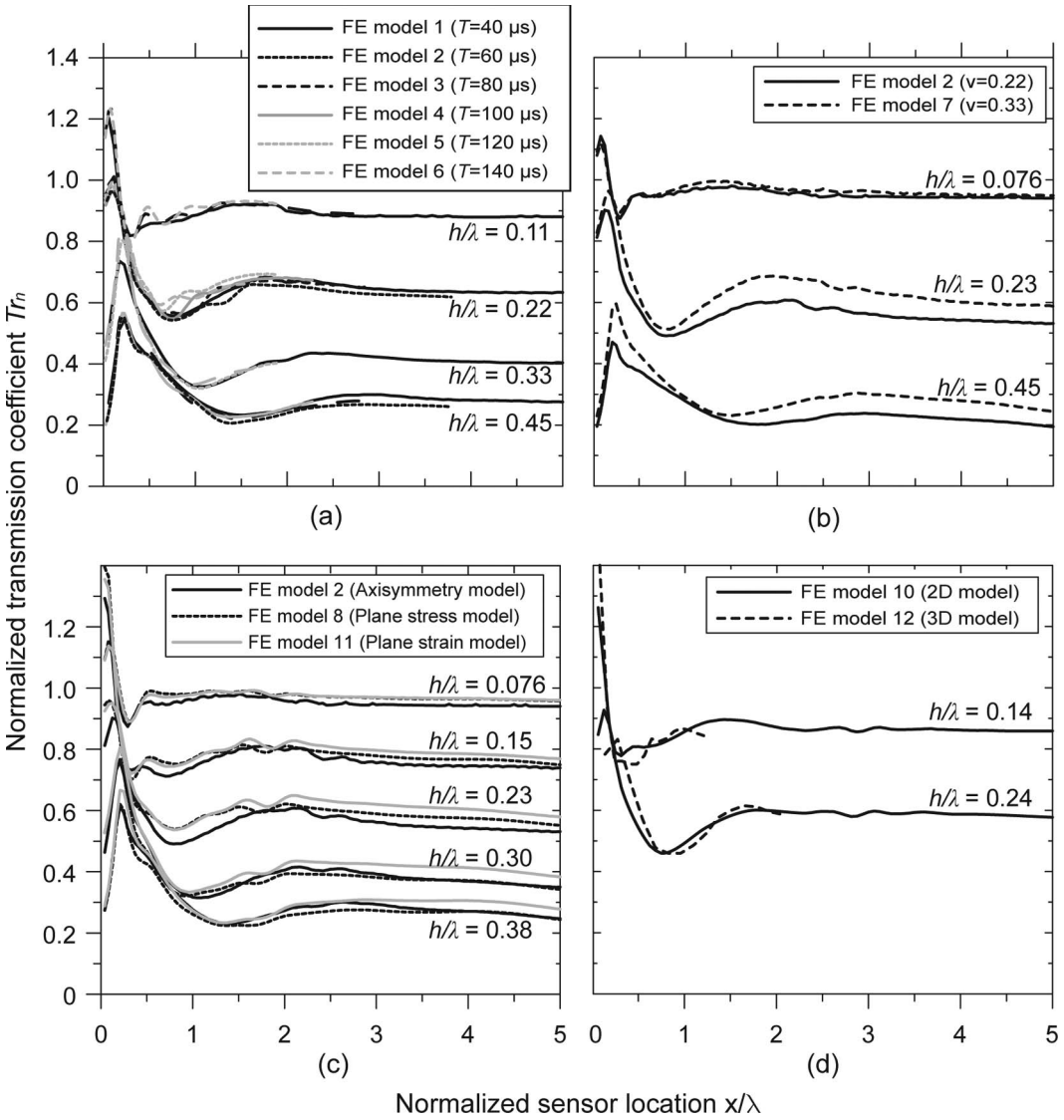

Fig. 8. Normalized transmission coefficient $\mathrm{Tr_n}$ versus normalized sensor location from a crack opening x/λ. All curves were obtained from parametric studies using FE models to investigate effects of various parameters on the variation of $\mathrm{Tr_n}$ with increasing x/λ. (a) Frequency contents of incident surface waves (T), (b) Poisson's ratio v of the solid media, (c) selection of element types, and (d) 2-D model versus 3-D model.

increasing x/λ, although frequency contents of the impact sources (T) are different. This result indicates that the $\mathrm{Tr_n}$ and x/λ relationship is mainly controlled by h/λ. The frequency bandwidth of the incident surface waves has little effect on it.

Fig. 8(b) shows the effect of Poisson's ratio v on the $\mathrm{Tr_n}$ and x/λ relation. The FE Models 2 ($v = 0.22$) and 7 ($v = 0.33$) have the same material properties and geometric conditions except for Poisson's ratios. $\mathrm{Tr_n}$ and x/λ relations for different h/λ (i.e., 0.076, 0.23, and 0.45) obtained from the FE Models 2 and 7 are depicted using solid lines and dashed lines, respectively. It is found that the model with the higher Poisson's ratio ($v = 0.33$) gives higher $\mathrm{Tr_n}$ than the model with the lower Poisson's ratio ($v = 0.22$) for the same x/λ. The effect of Poisson's ratio increases with increasing h/λ. However, the $\mathrm{Tr_n}$ versus x/λ curves (i.e., signal enhancement, and oscillation) are similar despite the different Poisson's ratios.

Fig. 8(c) shows the $\mathrm{Tr_n}$ and x/λ relations for various h/λ (0.076, 0.15, 0.23, 0.30, and 0.38) obtained from the axisymmetric model (model 2), the plane stress model (model 8), and plane strain model (model 11). As shown in Table II, FE model 2 is the same as model 8 and model 11 except for the element types. The results in Fig. 8(c) demonstrate that variation of transmission coefficients from three different models shows fairly good agreement with each other in the near-scattering field of a surface-breaking crack ($x/\lambda < 2$), especially between plane strain and plane stress models. For three cases, $\mathrm{Tr_n}$ converges to a constant value with increasing x/λ.

In addition, the combined effects of critical material properties (v, E, and ρ) and element types on $\mathrm{Tr_n}$ and x/λ relations are also shown in Fig. 6. Note that the material properties for FE Model 2 correspond to a normal concrete, whereas those of FE Model 10 are for Plexiglas. Despite of the difference in material properties, $\mathrm{Tr_n}$ and

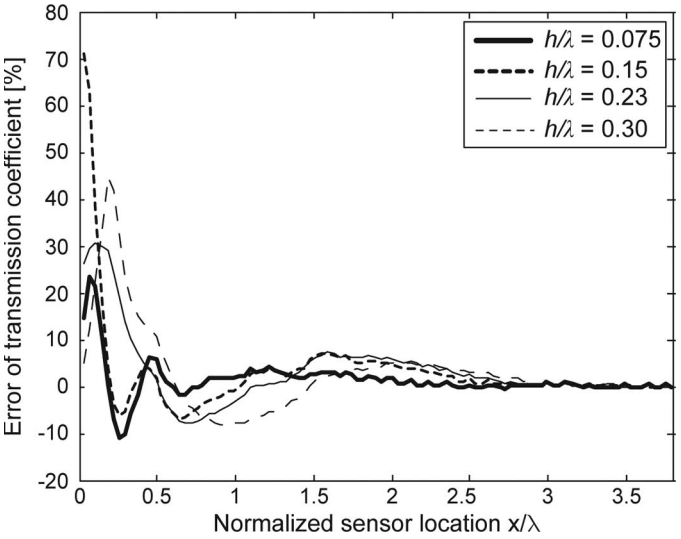

Fig. 9. Errors of transmission coefficient as a function of the normalized sensor-to-crack distance (x/λ).

x/λ relations from these two models show good agreement with each other.

Fig. 8(d) compares $\mathrm{Tr_n}$ variation with sensor location x/λ curves obtained from 2-D (FE model 10) and 3-D models (FE model 12) for two crack depths $h/\lambda = 0.14$ and 0.24. Results from 2-D models were extended to $x/\lambda = 5$, whereas results from 3-D models were presented in the range of $x/\lambda < 2$ because of the size limitation of the 3-D models. Nevertheless, in the near-scattering field of a surface-breaking crack, results from 3-D models show good agreement with those from 2-D models. This demonstrates the validity of the 2-D models in this study.

Based on this parametric study, although many parameters affect the near-field scattering by a surface-breaking crack, the most critical parameters for determination of transmission coefficients are the crack depth h/λ and sensor location x/λ.

V. Guidelines on Selecting Sensor Locations in the SWT Method

The experimental studies and numerical simulations show that the signal enhancement and oscillatory behaviors of transmission coefficients are due to the near-field interaction of surface waves with the surface-breaking crack, which makes it difficult to obtain consistent transmission measurements in the near-field region. Cheng and Achenbach [12] proposed $x > 5\lambda$ as an approximate far-field guideline. However, in practice, this criterion is not always satisfied because of the limitations of specimen geometry. In this section, the errors caused by near-field effects in surface wave transmission measurements are evaluated through comparison with the results from far-field measurements. A guideline for selecting sensor locations is proposed based on error analysis.

Fig. 9 shows errors of transmission coefficient (EOT) caused by the near-field effect. In this study, EOT is defined as follows:

$$\mathrm{EOT}\,(h/\lambda, x/\lambda)[\%] = \frac{\mathrm{Tr_n}(h/\lambda, x/\lambda) - \mathrm{Tr_n}(h/\lambda, \infty)}{\mathrm{Tr_n}(0, \infty)} \times 100, \tag{7}$$

where $\mathrm{Tr_n}$ is the normalized transmission coefficients determined by using (3). EOT indicates the deviation of transmission coefficients measured at a specific sensor location from those measured in the far-field. The converged transmission coefficients mentioned in the previous section (see also Fig. 8) were regarded as the far-field measurement. The negative and positive sign of EOT indicate under- and over-estimation of transmission measurement, respectively.

Fig. 9 reveals that EOT is less than 5% for $x/\lambda > 2.0$. In the h/λ range of interest for crack depth estimation, i.e., $h/\lambda = 0.1$ to 0.3, the sensitivity of transmission function with respect to h/λ is greater than 2.0. Therefore, 5% error in the transmission measurement will lead to less than 2.5% error in h/λ estimation. Note that the sensitivity of the transmission function was obtained from the first derivative of the transmission function for surface waves across a surface-breaking crack suggested by Angel and Achenbach [10] with respect to the h/λ. In contrast, EOT varies within $\pm$ 10% when sensors are located between 0.5λ and 1.5λ from the crack opening ($0.5 < x/\lambda < 1.5$). Likewise, the error of h/λ is less than approximately 5% when h/λ is in the range from 0.1 to 0.3.

VI. Conclusions

The near-field scattering of surface waves caused by a surface-breaking crack is thoroughly investigated within the crack depth range of $0 < h/\lambda < 1/3$, which is sensitive to crack depth variation in the surface wave transmission method. Conclusions based on experimental studies and numerical simulations are drawn as follows:

1) Results from experimental studies and numerical simulations reveal that the transmission function ($\mathrm{Tr_n}$) of surface waves across a surface-breaking crack is affected not only by the crack depth h, and the wavelength of incident surface waves λ, but also by the sensor location from the crack opening x. Strong signal enhancement and oscillation of transmission coefficient are observed when sensors are located within 0.5λ of the crack opening. The oscillatory behavior of transmission coefficients becomes weaker as sensors are located approximately 1.5λ from the crack, and almost disappears when sensors are 2.0λ away from the crack.
2) Numerical simulations and experimental measurements show good agreement in surface wave transmission function calculation, especially for the Plexiglas specimens, a type of homogeneous material. For the concrete specimens, material heterogeneity and wave scattering by coarse aggregates in concrete decrease the agreement between numerical and experimental

transmission curves in the near-scattering field. The degree of agreement improves in the far-field.

3) To obtain reliable and consistent transmission coefficients, measurements should be performed in the far-field. Analyses in this study show that surface wave transmission coefficients converge to a constant value in the far-field for large x/λ. Transmission coefficients in far-field measurements also converge to the analytical solution based on steady-state analysis given by Angel and Achenbach [10].
4) Near-field effects induce errors in surface wave transmission measurements. Error analysis shows that the error in transmission coefficient depends on the normalized sensor locations (x/λ). When $x/\lambda > 2.0$, the error is around 5%, and the corresponding error in crack depth estimation is about 2.5% of the wavelength λ of incident surface waves.

References

[1] I. A. Viktorov, *Rayleigh Waves and Lamb Waves-Physical Theory and Application*. New York: Plenum, 1967.

[2] G. S. Kino, "The application of reciprocity theory to scattering of acoustic waves by flaws," *J. Appl. Phys.*, vol. 49, no. 6, pp. 3190–3199, 1978.

[3] B. A. Auld, "General electromechanical reciprocity relations applied to the calculation of elastic wave scattering coefficients," *Wave Motion*, vol. 1, no. 3, pp. 3–10, 1979.

[4] J. D. Achenbach, A. K. Gautesen, and D. A. Mendelsohn, "Ray analysis of surface-wave interaction with edge crack," *IEEE Trans. Sonics Ultrason.*, vol. SU-27, no. 3, pp. 124–129, 1980.

[5] J. J. W. Tien, B. T. Khuri-Yakub, G. S. Kino, D. B. Marshall, and A. G. Evans, "Surface acoustic wave measurements of surface cracks in ceramics," *J. Nondestruct. Eval.*, vol. 2, no. 3–4, pp. 219–229, 1981.

[6] R. L. Jungerman, B. T. Khuri-Yakub, and G. S. Kino, "Characterization of surface defects using a pulsed acoustic laser probe," *Appl. Phys. Lett.*, vol. 44, no. 4, pp. 392–393, 1984.

[7] J. A. Cooper, R. A. Crosbie, R. J. Dewhurst, A. W. McKie, and S. B. Palmer, "Surface-acoustic wave interactions with cracks and slots: A noncontacting study using lasers," *IEEE Trans. Ultrason. Ferroelectr. Freq. Control*, vol. UFFC-33, no. 5, pp. 462–470, 1986.

[8] J. D. Achenbach, L. M. Keer, and D. A. Mendelsohn, "Elastodynamic analysis of an edge crack," *J. Appl. Mech.*, vol. 47, no. 3, pp. 551–556, 1980.

[9] D. A. Mendelsohn, J. D. Achenbach, and L. M. Keer, "Scattering of elastic waves by a surface-breaking crack," *Wave Motion*, vol. 2, no. 3, pp. 277–292, 1980.

[10] Y. C. Angel and J. D. Achenbach, "Reflection and transmission of obliquely incident Rayleigh waves by a surface-breaking crack," *J. Acoust. Soc. Am.*, vol. 75, no. 2, pp. 313–319, 1984.

[11] C. H. Yew, K. G. Chen, and D. L. Wang, "An experimental study of interaction between surface waves and a surface breaking crack," *J. Acoust. Soc. Am.*, vol. 75, no. 1, pp. 189–196, 1984.

[12] A. Cheng and J. D. Achenbach, "A roller device to scan for surface-breaking cracks and to determine crack depth by a self-calibrating ultrasonic technique," *Res. Nondestruct. Eval.*, vol. 7, no. 4, pp. 185–194, 1996.

[13] J. D. Achenbach, I. N. Komsky, Y. C. Lee, and Y. C. Angel, "Self-calibrating ultrasonic technique for crack depth measurement," *J. Nondestruct. Eval.*, vol. 11, no. 2, pp. 103–108, 1992.

[14] B. Masserey and E. Mazza, "Analysis of the near-field ultrasonic scattering at a surface crack," *J. Acoust. Soc. Am.*, vol. 118, no. 6, pp. 3585–3594, 2005.

[15] G. Hevin, O. Abraham, H. A. Petersen, and M. Campillo, "Characterization of surface cracks with Rayleigh waves: A numerical model," *NDT Int.*, vol. 31, no. 4, pp. 289–298, 1998.

[16] J. S. Popovics, W.-J. Song, M. Ghandehari, K. V. Subramaniam, J. D. Achenbach, and S. P. Shah, "Application of surface wave transmission measurements for crack depth determination in concrete," *ACI Mater. J.*, vol. 97, no. 2, pp. 127–135, 2000.

[17] W.-J. Song, J. S. Popovics, J. C. Aldrin, and S. P. Shah, "Measurement of surface wave transmission coefficient across surface-breaking cracks and notches in concrete," *J. Acoust. Soc. Am.*, vol. 113, no. 2, pp. 717–725, 2003.

[18] S.-H. Kee and J. Zhu, "Using air-coupled sensors to evaluate the depth of a surface-breaking crack in concrete," *J. Acoust. Soc. Am.*, vol. 127, no. 3, pp. 1279–1287, 2010.

[19] J. L. Blackshire and S. Sathish, "Near-field ultrasonic scattering from surface-breaking cracks," *Appl. Phys. Lett.*, vol. 80, no. 18, pp. 3442–3444, 2002.

[20] R. S. Edwards, X. Jian, Y. Fan, and S. Dixon, "Signal enhancement of the in-plane and out-of-plane Rayleigh wave components," *Appl. Phys. Lett.*, vol. 87, no. 19, art. no. 194104, 2005.

[21] X. Jian, S. Dixon, and N. Guo et al., "Rayleigh wave interaction with surface-breaking cracks," *J. Appl. Phys.*, vol. 101, art. no. 064906, 2007.

[22] N. Ryden and C. Park, "Surface waves in inversely dispersive media," *Near Surface Geophys.*, vol. 2, no. 4, pp. 187–197, 2004.

[23] A. Zerwer, M. A. Polak, and J. C. Santamarina, "Wave propagation in thin Plexiglas plates; Implications for Rayleigh waves," *NDT Int.*, vol. 33, no. 1, pp. 33–41, 2000.

[24] J. Zhu, "Non-contact NDT of concrete structures using air-coupled sensors," Ph.D. dissertation, Dept. of Civil and Environmental Engineering, the University of Illinois at Urbana, Urbana, IL, 2005.

[25] L. Eisner and R. W. Clayton, "A reciprocity method for multiple-source simulations," *Bull. Seismol. Soc. Am.*, vol. 91, no. 3, pp. 553–560, 2001.

[26] *Analysis User's Manual, v. 6.7.1*, ABAQUS Inc., Providence, RI, 2007.

[27] D. Alleyne and P. Cawley, "A two-dimensional Fourier transform method for the measurement of propagating multimode signals," *J. Acoust. Soc. Am.*, vol. 89, no. 3, pp. 1159–1168, 1991.

[28] J. H. Kim and H.-G. Kwak, "Nondestructive evaluation of elastic properties of concrete using simulation of surface waves," *Comput.-Aided Civ. Infrastruct. Eng.*, vol. 23, no. 8, pp. 611–624, 2008.

[29] F. E. Richart, R. D. Woods, and J. R. Hall, *Vibration of Soils and Foundations*, Englewood Cliffs, NJ: Prentice-Hall, 1970.

[30] M. Hirao, H. Fukuoka, and Y. Miura, "Scattering of Rayleigh surface waves by edge cracks: Numerical simulation and experiment," *J. Acoust. Soc. Am.*, vol. 72, no. 2, pp. 602–606, 1982.

Seong-Hoon Kee received the B.S. degree in architectural engineering and the M.S. degree in structural engineering from Hanyang University, Seoul, South Korea, in 2001 and 2005, respectively.

Since 2006, he has been a graduate student at the University of Texas, Austin, in civil engineering. His current research involves non-destructive testing and structural health monitoring of concrete structures.

Jinying Zhu received her Ph.D. degree in civil engineering from the University of Illinois at Urbana-Champaign, Urbana, IL, in 2006. She is currently an assistant professor at the University of Texas at Austin. Her current research interests focus on developing rapid NDT techniques for concrete structures, and characterizing cement material properties using innovative sensors. She is a member of American Concrete Institute (ACI) and a recipient of ACI-James Instrument Research Award.